Hybrid electrons in the trimerized GaV 4 O 8 .

Cintli Aguilar-Maldonado, Olivier Mentré, Alexander A Tsirlin, Clemens Ritter, Aleksandr Missiul, Francois Fauth, Angel M Arévalo-López

COMMUNICATION

Hybrid electrons in the trimerized GaV_4O_8.

Cintli Aguilar-Maldonado[a], Olivier Mentré[a], Alexander A. Tsirlin[b], Clemens Ritter[c], Aleksandr Missiul[d], Francois Fauth[d] and Angel M. Arévalo-López[a]*.

Received 00th January 20xx,
Accepted 00th January 20xx

DOI: 10.1039/x0xx00000x

Mixed-valent transition-metal compounds display complex structural, electronic and magnetic properties, which often intricately coexist. Here, we report the new ternary oxide GaV_4O_8, a structural sibling of skyrmion-hosting lacunar spinels. GaV_4O_8 contains a vanadium trimer and an original spin-orbital-charge texture that forms upon the structural phase transition at T_S = 68 K followed by the magnetic transition at T_N = 35 K. The texture arises from the coexistence of orbital molecules on the vanadium trimers and localized electrons on the remaining vanadium atoms. Such hybrid electrons create opportunities for novel types of spin, charge, and orbital order in mixed-valent transition-metal compounds.

1 Introduction

Transition-metal compounds with molecular clusters open a new dimension in the physics and chemistry of strongly correlated electronic systems.[1] For instance, the lacunar spinel GaV_4S_8, where every second A-site ion is removed from a normal AM_2X_4 spinel, presents orbitally driven ferroelectricity and a Néel-type skyrmion lattice from a cooperative Jahn-Teller distortion at T_S = 42 K and a magnetic transition at T_C = 13 K respectively, defining a vanadium-based breathing pyrochlore framework.[2,3,4] The same happens with its GaV_4Se_8 analogue, showing a T_S = 41 K and T_C = 17.5 K.[5,6] However, no lacunar spinel has been reported in vanadium oxides. GaV_2O_4, the closest analogue of these chalcogenides reported to date, was recently studied and displays coexisting $[V_3]^{9+}$ trimer and $[V_4]^{8+}$ tetramer clusters ("orbital molecules") below a charge-ordering transition at T_{CO} = 415 K, whereas no magnetic long-range order has been observed.[7]

$BaV_{10}O_{15}$ and V_4O_7 are other mixed valent vanadium oxides which respectively present tri- and dimerization and metal-insulator transitions due to charge and orbital orderings. [8,9] However, their magnetic structures have never been solved and thus the magnetism of partially localized (*i.e.* hybrid) electrons discussed in here could not be probed.

As a rule of thumb, molecular-orbital crystals with an even number of electrons show non-magnetic or singlet-based states, e.g. $LiVO_2$,[10] while crystals with an odd number of electrons behave as molecular or even quantum magnets, such as $LiZn_2Mo_3O_8$ with a spin ½ per Mo trimer and isostructural to GaV_4O_8. Its localized spin remains disordered down to 50 mK and possibly forms a spin-liquid state.[11] GaV_4S_8, with six out of the seven electrons involved in the covalent bonds inside the tetrahedral molecule, also shows residual spin ½ that remains uniformly distributed over the V_4 molecule even in the Jahn-Teller-distorted ferromagnetic-ferroelectric low-temperature phase.[12,13]

In this letter, we report the new GaV_4O_8 compound, the oxide analogue of the skyrmion-hosting vanadium-based lacunar spinel chalcogenides. It nevertheless shows a different flavour of the closed-packed crystal structure and the most drastic $[V_3]^{10+}$ trimerization, that gives rise to the hybrid behaviour of antiferromagnetic (AFM) partially localized moments and covalent molecular-cluster vanadium electrons. It also opens the path for new structurally related oxychalcogenides with exotic properties.

2 Methods

Polycrystalline GaV_4O_8 was synthesised from a stoichiometric mixture of Ga_2O_3, V_2O_3 and VO_2 in a vacuum sealed quartz ampule heated at 1150 °C for 24 hours. V_2O_3 was prepared from reduction of V_2O_5 under hydrogen at 700 °C and VO_2 from a 1:1 V_2O_3:V_2O_5 mixture at 700 °C. Small single crystals of doped

[a] Université Lille Nord de France, UMR 8181 CNRS, Unité de Catalyse et de Chimie du Solide (UCCS USTL), F-59655 Villeneuve d'Ascq, France. angel.arevalo-lopez@univ-lille.fr.
[b] Experimental Physics VI, Center for Electronic Correlations and Magnetism, University of Augsburg, 86159 Augsburg, Germany
[c] Institut Laue-Langevin, Avenue des Martyrs 71, Grenoble Cedex, France.
[d] CELLS-ALBA Synchrotron, 08290 Cerdanyola, Barcelona, Spain.
† Footnotes relating to the title and/or authors should appear here.
Electronic Supplementary Information (ESI) available: DFT calculations and further characterisation, tables and figures. See DOI: 10.1039/x0xx00000x

$Ga_{1+x}V_{4-x}O_8$ were obtained via chemical vapor transport for crystal determination as detailed in SI (CSD-2059095). Preliminary laboratory X-ray powder diffraction patterns were collected using Cu-Kα radiation on a Bruker D8 Advance diffractometer in the $5 < 2\Theta < 90^o$ range. Synchrotron XRD data were collected at low temperature using the BL04 - MSPD beamline (λ = 0.41285 Å) at ALBA, Barcelona.[14,15] Neutron powder diffraction (NPD) data were taken between 1.5 and 50 K every 3 K using the D1B beamline at the ILL, Grenoble (λ = 2.52 Å). In order to resolve the magnetic structure, 8-hour long scans were mandatory at 1.5 K and 50 K in D20 at ILL (λ = 2.41 Å) for the required statistics. Rietveld refinements were done with Fullprof Suite.[16]

Magnetisation, heat capacity and resistivity measurements were obtained from experiments in a Quantum Design PPMS 9T Dynacool. Magnetic susceptibilities were measured from 2 K to 300 K under a $\mu_0 H$ = 0.1 T magnetic field using zero- (ZFC) and field-cooling (FC) procedures. Magnetisation versus field isotherms were measured between -9 and 9 T. Van-der-Paw method was used for resistivity measurements.

Density-functional band-structure calculations were performed in the FPLO code[17] using local density approximation[18] for the exchange-correlation potential. Correlation effects in the V 3*d* shell were considered on the mean-field DFT+*U* level with the on-site Coulomb repulsion parameter U_d = 4 eV and Hund's coupling J_d = 1 eV.[19]

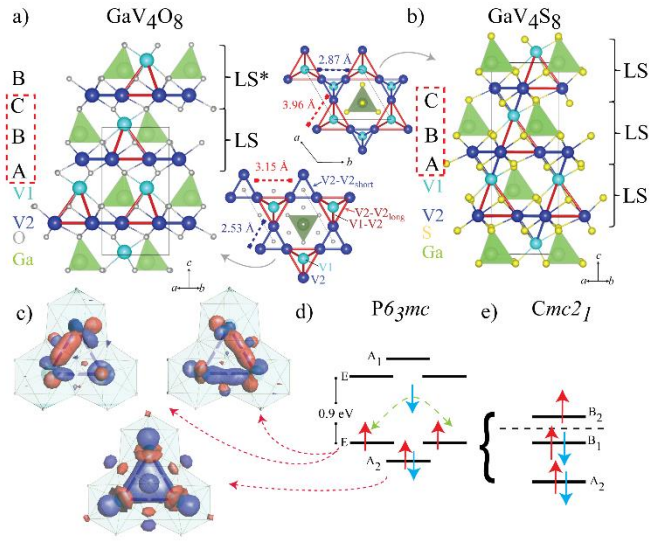

Figure 1 a) Crystal structure of GaV_4O_8 consisting of alternating layers of corner-sharing GaO_4 tetrahedra with $V1O_6$ octahedra and $V2O_6$ octahedra on a breathing *Kagomé* layer. It shows an ABCB stracking sequence which defines LSLS* blocks as compared to b) structure of GaV_4S_8 with an (ABC) stacking and $(LS)_3$ blocks in the rhombohedral phase as detailed in the text. c) GaV_4O_8 extended Hückel results for the corresponding HOMO levels in the $V2_3O_{13}$ triangle with 5 electrons showing the trimerized cluster and the E double-degenerate level in d). The energy gap with the LUMO levels is 0.9 eV. e) Removal of the orbital degeneracy due to a Jahn-Teller transition at low temperatures from $P6_3mc$ to $Cmc2_1$.

3 Results

GaV_4O_8 crystallizes with an oxygen (ABCB) close packing framework along the c direction forming a (LS)(LS)* modular sequence (a = 5.696(4) Å, c = 9.387(4) Å, $P6_3mc$ polar space group). LS stands for Lacunar Spinel blocks, formed by corner sharing $[GaO_4]$ tetrahedra and $[V1O_6]$ octahedra in one layer and edge-sharing $[V2O_6]$ octahedra in a breathing Kagomé-lattice in another layer (Ga, V1 and V2 have 2b, 2b and 6c Wyckoff positions respectively). (LS)* blocks are mirrored *in-plane* as shown in Figure 1a. It differs from its chalcogenide analogues by their $(ABC)_2$ packing, giving a $(LS)_3$ block sequence in their rhombohedral phase (a = 6.799 Å and c = 16.782 Å for GaV_4S_8, $R3m$ space group)[20] as shown in Figure 1b. Moreover, due to this stacking difference and changes in the V-V distances, the vanadium breathing pyrochlore lattice of the sulphide (V-V_{short} = 2.87 Å, V-V_{long} = 3.96 Å) is broken in the oxide ($V2$-$V2_{short}$ = 2.535(2) Å in V_3 triangles, and 3 x $V2$-$V2_{long}$ = 3.161(3) Å plus apical $V1$-$V2$ = 3.154(2) Å in V_4 tetrahedra).

The average formal oxidation states are $Ga^{3+}V_4^{3.25+}O_8^{2-}$. Bond valence sum calculations via an interpolation method[21] result in +3.17 for V1 and +3.37 for V2 suggesting a +3.33 mixed valence state in the Kagomé layer.

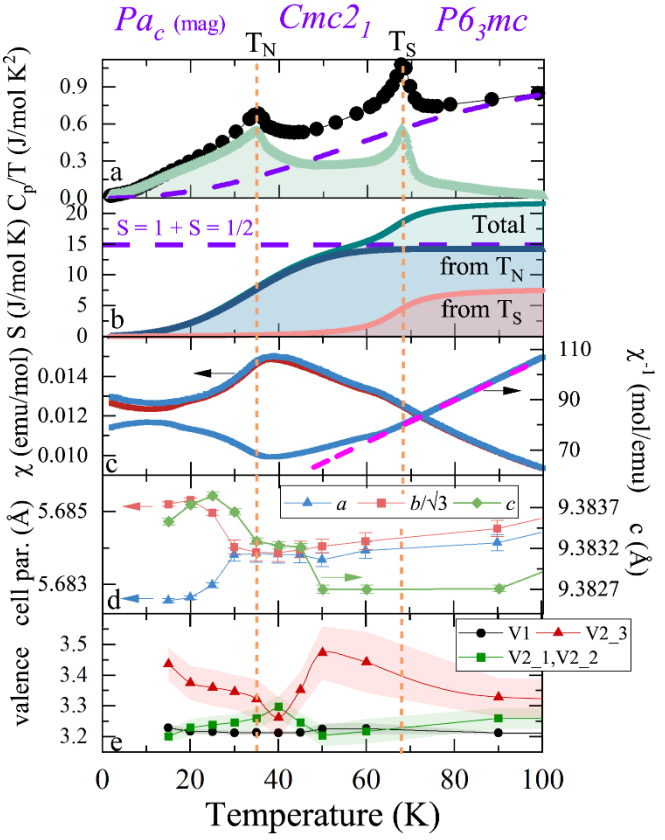

Figure 2. a) Specific heat divided by temperature (black dots) along with magnetic (green area) and lattice contributions (dashed purple line). b) Calculated entropy with the ideal value for a system with S = ½ and S = 1 contributions as a horizontal broken line. c) Temperature dependence of the direct and inverse magnetic susceptibility in zero-field (red) and field cooled (blue) protocols and Curie-Weiss fit above 100 K (dashed pink line). d) Orthorhombic cell parameters behaviour at low temperature, uniaxial zero and negative thermal expansion along c is observed below T_S and divergence between a and $b/\sqrt{3}$ below T_N. e) Vanadium valence obtained from BVS calculations from refinements in the orthorhombic $Cmc2_1$ cell. Vertical orange dashed lines mark T_N = 35 K and T_S = 68 K transitions. The labels at the top correspond to the space groups above and below T_S ($P6_3mc$ and $Cmc2_1$) and below T_N (Pa_c being the magnetic one).

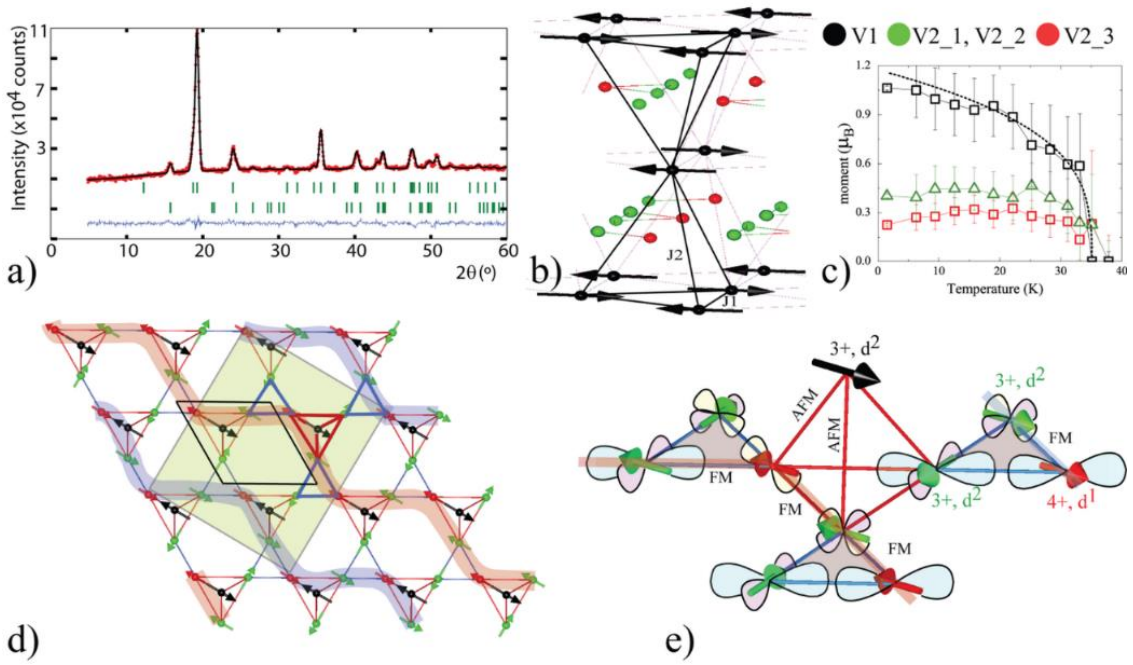

Figure 3 Magnetic structure for GaV_4O_8. a) Rietveld fit to the NPD 1.5 K – 50 K difference pattern. Second row of Bragg tick marks refers to the V_3O_5 magnetic structure. b) V1 hcp lattice as magnetic backbone for GaV_4O_8. c) Thermal evolution of the magnetic moments. Fit of V1 moments to a critical law is shown as a dashed line. d) Charge-orbital texture; green and black arrows represent V^{3+}; red arrows, V^{4+}. Shaded blue/red chains represent ferromagnetic short-long V^{4+}-V^{3+}-V^{4+} zig-zag chains AFM coupled. e) Charge, orbital and spin order for GaV_4O_8. Shaded triangles represent the trimerized V2 atoms.

The V2-V2 intracluster distance is much shorter than the localized-itinerant critical V-V distance of R_c = 2.90 Å and can be attributed to the formation of a trimer molecule.[22] From extended Hückel molecular orbital (M.O.) calculations (Fig. 1c), the $V2_3O_{13}$ cluster forms a triplet with four out of the five *d* electrons (2 x d^2 from 2 x V^{3+} plus 1 x d^1 from V^{4+}) ~~electrons~~ into V2-V2 covalent bonds and holding together the trimer. The single unpaired electron (S = ½) favours a Jahn-Teller instability while remaining in the double-degenerate M.O. level (E irreducible representation) and thus a structural transition occurs at low temperature as described below (Fig 1d and 1e). This is also supported through DFT calculations as shown in SI. The other two V valence electrons of the GaV_4O_8 formula unit remain unpaired in the isolated $V1^{3+}O_6$ (S = 1) octahedra. GaV_4O_8 presents an insulating behaviour with a ΔE = 0.24(1) eV activation energy (Fig. S4).

GaV_4O_8 is isostructural to the $A_2Mo_3O_8$ family of compounds but, as shown below, with a very different magnetism since those do not contain magnetic-metal ions beyond the trimer, *e.g.* $Zn_2Mo_3O_8$,[23] or the trimer itself is not magnetic as in $Fe_2Mo_3O_8$.[24] Thus, making GaV_4O_8 a natural bridge between 2D trimerized Kagomé lattices, *e.g.* $A_2Mo_3O_8$ family, and 3D breathing pyrochlores, such as lacunar spinels with tetrahedral units.

Two sharp λ-type transitions at T_S and T_N were observed in the heat capacity measurements (Fig. 2a). After removal of the lattice contribution, the magnetic entropy determined by integrating the specific heat divided by temperature (C_m/T) is shown in Fig. 2b. The recovered entropy at T_N agrees well with the magnetic contribution from coexisting S = ½ and S = 1 (*i.e.* R*ln(6)), as inferred from the Curie-Weiss fit (Fig 2c). The additional entropy of 7.4 J / mol K recovered around T_S should then have a main structural origin, and indeed no magnetic intensity was detected in neutron diffraction above T_N, vide infra. The presence of two transitions resembles the situation found in GaV_4S_8 where T_N = 12.7 K and where at T_{JT} = 44 K a structural transition takes place.[25] Following this analogy, the low temperature synchrotron data were used to search for a symmetry reduction below T_S. The trigonal cell is preserved within error but a uniaxial zero and later a negative thermal expansion occurs along *c*, a signature of the structural transition. Only below T_N a clear orthorhombic lattice distortion is observed, due to remaining thermal excitation of the > T_S configuration. Treating all the data in $Cmc2_1$ (Figure 2d), the unique orthorhombic subgroup of $P6_3mc$, splits the V2 sites into V2_1(V2_2) and V2_3 (8b and 4a Wyckoff positions respectively), indicative of a charge ordering with the thermal variations of interpolated BVS changing from +3.24(2) and +3.29(6) at 90 K to +3.15(3) and +3.44(5) for V2_1 and V2_3, respectively, at 50 K, which is the temperature where the difference is maximum before the structural flexibility becomes apparent. The BVS for V1 (+3.22(1)) remains almost constant across the two transitions (Figure 2e).

Neutron powder diffraction data show additional Bragg reflections below T_N with the intensity increasing smoothly on cooling (Fig. S7). These extra reflections were consistent with a magnetic unit cell commensurate with the nuclear crystal structure and described by the magnetic propagation vector k = [¼ ¼ 0] (Λ point of the first Brillouin zone), unusual for a hexagonal cell. ISODISTORT[26,27] was used to determine the possible magnetic structures and space group. The final fit was obtained with the mΛ2 irreducible representation in a {(2, 2, 0),

(-1, 1, 0), (2, 2, 1)} supercell with the monoclinic Pa_c magnetic space group (7.27).

The magnetic structure has four independent cations with moments confined to the *ab* plane (Fig. 3). The largest moment of 1.06(1) μ_B is observed on the V1 site, whereas much lower moments of 0.2-0.4 μ_B were obtained for the three-independent magnetic V2 sites, where trimer molecules are formed. The V1 moments alone form an *hcp* magnetic lattice with two main couplings, the in-plane J_1 and out-of-plane J_2 (Fig. 3b). Our DFT calculations suggest that both couplings are antiferromagnetic (J_1 ~ 6 K, J_2 ~ 7 K) and cause strong frustration, although a collinear state with two up- and two down-spins on each $V1_4$ tetrahedron should eventually form[28,29] in accord with the experimental magnetic structure. This magnetic model predicts an ordering temperature of 22 K and reproduces the order of magnitude of the experimental T_N. Thus, the *hcp* V1 lattice can be considered as the backbone for the magnetic structure of GaV_4O_8.

Weaker magnetic moments on the V2 sites are nevertheless essential to achieve a complete description of the neutron data. This site splits in three independent V2 positions in the Pa_c magnetic space group. Nearly equal moments were obtained for the structurally equivalent V2_1 and V2_2, reminiscent of the structural orthorhombicity, and finally our best fit returns 0.40(1) μ_B for these and 0.225(7) μ_B for V2_3 (R_{mag} = 8.87%), see Fig. 3c and 3d. This confirms that a structural instability occurs at T_S and results in an unequal distribution of spin density inside the trimer molecule. The local moment values are well scaled by the BVS given above. They indicate charge order ultimately seen as covalently bonded V^{3+} at the V2_1 and V2_2 sites (higher moment) and V^{4+} at the V2_3 site (lower moment) (Fig. 3c). Besides BVS, this charge distribution is consistent with the magnetic moments from DFT (1.78 μ_B for V1, 1.3-1.5 μ_B for V2_1-V2_2 and 0.99 μ_B for V2_3) and can explain qualitatively the nature of magnetic order in the *ab* plane. Empty orbitals favour ferromagnetic direct- (intra-trimer) or super- (inter-trimer) exchanges between adjacent sites in a V^{4+}-V^{3+}-V^{4+} zig-zag short-long ferromagnetic chains as shown by red (↑) and blue (↓) stripes on Figure 3d, in accordance with Goodenough-Kanamori-Anderson exchange rules or the Kugel-Khomskii orbital scheme resulting in a complex charge-orbital-spin texture as detailed in Figure 3e.[30,31,32] The AFM couplings around the remaining V2 spins in between the stripes are frustrated and minimized by a perpendicular alignment to the other spins.

4 Conclusion

Our results pinpoint the principal difference between the new GaV_4O_8 and the previously known chalcogenides GaV_4S_8 and GaV_4Se_8. This difference may stem from the fact that each edge of the V4 tetrahedron is "decorated" with a ligand atom. Oxygen appears too small to be compatible with the regular tetrahedron and causes its distortion toward a trigonal pyramid. Nevertheless, all three GaV_4X_8 compounds feature molecular units of the vanadium atoms and show a structural instability followed by the onset of magnetic order, but only in the oxide case the structural instability is accompanied by a charge re-distribution and results in a complex charge-orbital-spin texture compared to the weakly perturbed ferromagnetic order in the chalcogenides. The origin of this unusual scenario may lie in the nature of the orbital molecule (V_4 *vs* V_3) that leaves behind the purely "magnetic", localized electrons of $V1^{3+}$ in the oxide compound.

This hybrid behaviour fills the gap between, on one hand, vanadium spinels with orbital molecules (GaV_2O_4, AlV_2O_4, GaV_4S_8) and, on the other hand, mixed-valence oxides that show a complete charge order at low temperatures (MgV_2O_4, ZnV_2O_4). It parallels the scenario of binary vanadium oxides, such as V_4O_7 with the dual behaviour of dimerized non-magnetic V^{4+} and antiferromagnetic V^{3+}, but in our case the electrons of the orbital molecule contribute also to the magnetic response and magnetic structure.[33,34,35,36] Most generally, such hybrid electrons create a natural avenue for tuning mixed-valence transition-metal compounds between the limits of single-site charge order and orbital molecules, e.g., in the mixed oxochalcogenides based on GaV_4O_8.

Altogether, the charge-orbital-spin texture in GaV_4O_8 shows a nice conundrum in condensed-matter physics, with the shortest V-V distance reported in oxides and thus delocalized moments inside the V_3O_{13} molecular trimer, and simultaneous electron localization with long-range charge and spin ordering.

Author contributions

The study was designed by AMAL. Sample synthesis and physical property characterisation was performed by CAM and AMAL with assistance from OM. CAM, CR, AM, FF and AMAL performed the diffraction experiments and analysis. DFT calculations were performed by AAT. The manuscript was written by AMAL with contributions from all other co-authors.

Conflicts of interest

There are no conflicts to declare.

Acknowledgments

We thank ALBA and the ILL for beamtime provided at BL04-MSPD and D1B+D20 beamlines respectively. AMAL thanks the ANR-AMANTS project (19-CE08-0002-01). CAM thanks CONACyT-Mexico for a post-doctoral fellowship (CVU 350841). Chevreul Institute (FR 2638), Region Hauts-de-France, and FEDER are acknowledged for funding the X-ray diffractometers and the PPMS magnetometer

References

1 E. Dorolti, L. Cario, B. Corraze, E. Janod, C. Vaju, H. J. Koo, E. Kan and M. H. Whangbo, *J. Am. Chem. Soc.*, 2010, **132**, 5704.

2 I. Kezsmarki, S. Bordacs, P. Milde, E. Neuber, L. M. Eng, J. S. White, H. M. Rønnow, C. D. Dewhurst, M. Mochizuki, K. Yanai, H. Nakamura, D. Ehlers, V. Tsurkan and A. Loidl, *Nat. Mater.*, 2015, **14**, 1116.

3 Z. Wang, E. Ruff, M. Schmidt, V. Tsurkan, I. Kézsmárki, P. Lunkenheimer and A. Loidl, *Phys. Rev. Lett*., 2015, **115**, 207601.
4 E. Ruff, S. Widmann, P. Lunkenheimer, V. Tsurkan, S. Bordács, I. Kézsmárki and A. Loidl, *Sci. Adv.*, 2015, **1**, 1500916.
5 Y. Fujima, N. Abe, Y. Tokunaga and T. Arima, *Phys. Rev. B*, 2017, **95**, 180410R.
6 S. Bordács, A. Butykai, B. G. Szigeti, J. S. White, R. Cubitt, A. O. Leonov, S. Widmann, D. Ehlers, H. A. K. Von Nidda, V. Tsurkan, A. Loidl and I. Kézsmárki, *Sci. Rep.*, 2017, **7**, 7584.
7 A. J. Browne, C. Lithgow, S. A. J. Kimber and J. P. Attfield, *Inorg. Chem.*, 2018, **57**, 2815.
8 T. Kajita, T. Kanzaki, T. Suzuki, J. E. Kim, K. Kato, M. Takata and T. Katsufuji, *Phys. Rev. B.*, 2010, **81**, 060405(R).
9 A. S. Botana, V. Pardo, D. Baldomir, A. V. Ushakov and D. I. Khomskii, *Phys. Rev. B.*, 2011, **84**, 115138.
10 H. F. Pen, J. Van den Brink, D. I. Khomskii and G. A. Sawatzky, *Phys. Rev. Lett.*, 1997, **78**, 1323.
11 J. P. Sheckelton, J. R. Neilson, D. G. Soltan and T. M. McQueen, *Nat. Mater.*, 2012, **11**, 493.
12 R. L. Dally, W. D. Ratcliff, L. Zhang, H. S. Kim, M. Bleuel, J. W. Kim, K. Haule, D. Vanderbilt, S. W. Cheong and J. W. Lynn, *Phys. Rev. B*, 2020, **102**, 014410.
13 A. Stefancic, S. J. R. Holt, M. R. Lees, C. Ritter, M. J. Gutmann, T. Lancaster and G. Balakrishnan, *Sci. Rep.* 2020, **10**, 9813.
14 F. Fauth, I. Peral, C. Popescu and M. Knapp, *Powder Diffraction* 2013, **28**, 360.
15 F. Fauth, T. Boer, F. Gil-Ortiz, C. Popescu, O. Vallcorba, I. Peral, D. Fulla, J. Benach, and J. Juanhuix, *Eur. Phys. J. Plus* 2015, **130**, 160.
16 J. Rodriguez-Carvajal, *Phys. B Condens. Matter* 1993, **192**, 55.
17 H. Eschrig, *Phys. Rev. B* 1999, **59**, 1743.
18 J. P. Perdew and Y. Wang, *Phys. Rev. B* 1992, **45**, 13244.
19 F. Weickert, N. Harrison, B. L. Scott, M. Jaime, A. Leitmae, I. Heinmaa, R. Stern, O. Janson, H. Berger, H. Rosner, A. A. Tsirlin, *Phys. Rev. B* 2016, **94**, 064403.
20 R. Pocha, D. Johrendt, R. Pöttgen, D. Haus and D. Mu, *Structure*, 2000, **64**, 2882.
21 J. P. Attfield, *Solid State Sci.*, 2006, **8**, 861.
22 J. B. Goodenough, G. Dutta and A. Manthiram, *Phys. Rev. B*, 1991, **43**, 10170.
23 C. C. Torardi and R. E. McCarley, *Inorg. Chem.*, 1985, **24**, 476.
24 Y. Wand, G. L. Pascut, B. Gao, T. A. Tyson, K. Haule, V. Kiryukhin and S-W. Cheong, *Sci. Rep.*, 2015, **5**, 12268.
25 S. Widmann, E. Ruff, A. Günther, H.-A. Krug von Nidda, P. Lunkenheimer, V. Tsurkan, S. Bordács, I. Kézsmárki and A. Loidl, *Philos. Mag.*, 2017, **97**, 3428.
26 H. T. Stokes, D. M. Hatch, and B. J. Campbell, ISODISTORT, ISOTROPY Software Suite, iso.byu.edu.
27 B. J. Campbell, H. T. Stokes, D. E. Tanner and D. M. Hatch, *J. Appl. Crystallogr.*, 2006, **39**, 607.
28 H. T. Diep, *Phys. Rev. B*, 1992, **45**, 2863.
29 D.-T. Hoang and H. T. Diep, *Phys. Rev. E*, 2012, **85**, 041107.
30 J. Kanamori, *J. Phys. Chem. Solids* 1959, **10**, 87.
31 J. B. Goodenough, *Phys. Rev.* 1955, **100**, 564.
32 K. I. Kugel and D. I. Khomskii, *Sov. Phys. - Uspekhi* 1982, **25**, 621.
33 M. Marezio, D. B. McWhan, P. D. Dernier and J. P. Remeika, *J. Solid State Chem.*, 1973, **6**, 419.
34 S. Kachi, K. Kosuge and H. Okinaka, *J. Solid State Chem.*, 1973, **6**, 258.
35 A. C. Gossard, J. P. Remeika, T. M. Rice, H. Yasuoka, K. Kosuge and S. Kachi, *Phys. Rev. B*, 1974, **9**, 1230.
36 Z. Hiroi, *Prog. Solid State Chem.*, 2015, **43**, 47.